Micro- and Macrostructural Studies of Sodium Deoxycholate Micellar Complexes in Aqueous Solutions

F. Lopez[†] and J. Samseth

Physics Department, Institute for Energy Technology (IFE), 2007 Kjeller, P.O. Box 40, Norway

K. Mortensen

Department of Solid State Physics, Risø National Laboratory, DK-4000 Roskilde, Denmark

E. Rosenqvist

Department of Vaccinology, National Institute of Public Health (NIPH), N-0462 Oslo, Norway

J. Rouch*

Centre de Physique Moléculaire Optique Hertzienne (CPMOH), URA 283 du CNRS, Université Bordeaux I, 351 Cours de la Libération, 33405 Talence, France

Received January 2, 1996. In Final Form: August 23, 1996[⊗]

We report on the self-aggregation patterns of sodium deoxycholate investigated successively by small-angle neutron scattering, quasi-elastic light scattering, viscosity, electrical conductivity, and time domain reflectometry as a function of pH, temperature, and detergent concentration. Experimental results reveal a rodlike association which seems to be strongly dependent on the pH and ionic strength. The radius and length of such conformations compare reasonably well with the dimensions of helical models and rods previously observed by small-angle X-ray scattering and electronic spin resonance. We also show the existence of two critical micellar concentrations. The lower one, corresponding to small primary micelles, is pH and temperature independent. The second one, which is strongly dependent on pH and temperature, leads to the formation of larger aggregates and in some cases to gelation. A sharp phase transition between solution and gel was observed at pH 7.5. The growth of the aggregate occurs along the rod's axis and is favored by a decreasing pH. At the opposite, the decrease of the micellar size along the rod's symmetry axis is favored by an increase of the pH.

Introduction

Sodium deoxycholate (NaDC) belongs to the bile salts category of steroid amphiphilic compounds, which do not have the usual polar head and nonpolar aliphatic tail in contrast with classical surfactants. Bile salts are synthesized in the liver from cholesterol and occur in the organism mainly as bile. They represent biological surfactants of vital importance in various phases of fat digestion, and their micellar properties still remain a subject of intense investigations. For instance, they have pharmaceutical importance as novel drug delivery systems and are also used to model small molecule interactions in membranes. Hjelm et al.[1,2] have extensively studied the morphology of some bile salt conjugates in aqueous mixtures of monoolein, lecithin, or dipalmitoylphosphatidylcholine (DPPC) by small-angle neutron scattering (SANS) and quasi-elastic light scattering (QELS). They have investigated the influence of the total lipid concentration on the structural conformation of these mixed colloidal dispersions. Their results provide undoubtedly the most interesting source of information about rodlike mixed micelles of glycocholate and glycochenodeoxycholate with lecithin or DPPC. However, literature about the conformation of NaDC micelles in aqueous solutions investigated by SANS and QELS remains scarce.

At their slightly alkaline pH, they are typical members of detergents which exhibit the very interesting properties of colloidal aggregation. The common bile salts are steroid nuclei which are saturated C24 acids derived from 5β-cholanic acid. The fusion between the A and B rings is of the cis (or 5β) configuration and may be of the trans (allo or 5α) configuration in some animal species. The B/C and C/D fusions are of the trans configuration, but it is worth noting that hydrophobic methyl groups protuding at positions C13 and C10 are cis (Figure 1). Bile acids may have one, two, or three hydroxyl groups localized in the equatorial or α positions and therefore protude beneath the relatively planer steroid skeleton. These hydrophilic elements are located at the C3, C7, and C12 positions and confer to these molecules a peculiar geometry divided into a hydrophilic concave surface on one side and a hydrophobic convex surface on the other side (Figure 2). Furthermore, the carboxyl group is equatorially orientated and contributes to the hydrophilicity of the molecule, as shown in Figure 1, representing the cholic acid structure.

Different models of micellization were proposed, and despite many experimental studies, the mechanism of micellar aggregation is still a matter of controversy. Small[3] proposed a spontaneous aggregation phenomenon of few bile salt molecules mediated by hydrophobic interactions. This mechanism would lead to the formation of larger secondary micelles via hydrogen bonding at higher surfactant concentration. Moreover, Oakenfull and

[†] On leave from CPMOH, Université Bordeaux I, 351 Cours de la Libération, 33405 Talence, France.

[⊗] Abstract published in *Advance ACS Abstracts,* November 15, 1996.

(1) Hjelm, R. P.; Schteingart, C. A. F.; Sivia, D. S. *J. Phys. Chem.* **1995**, *99*, 16395−16406 and references therein.

(2) Hjelm, R. P.; Alkan, M. H.; Thiyagarajan, P. *J. Phys. Chem.* **1992**, *96*, 8653−8661; *Mol. Cryst. Liq. Cryst.* **1990**, *180A*, 155−164.

(3) Small, D. M. *The Bile Acids*; Plenum Press: New York, 1971; Vol. 1.

S0743-7463(96)00006-6 CCC: $12.00

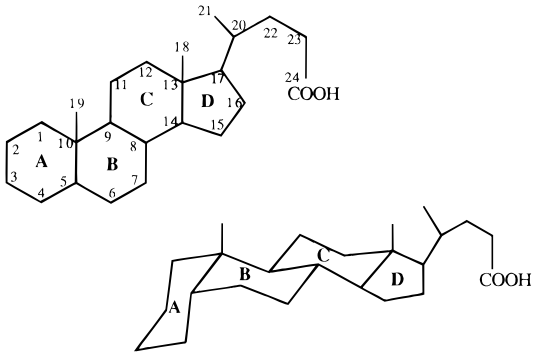

Figure 1. Structure formula of cholic acid indicating respectively the hydrophilic and hydrophobic parts of the molecule.

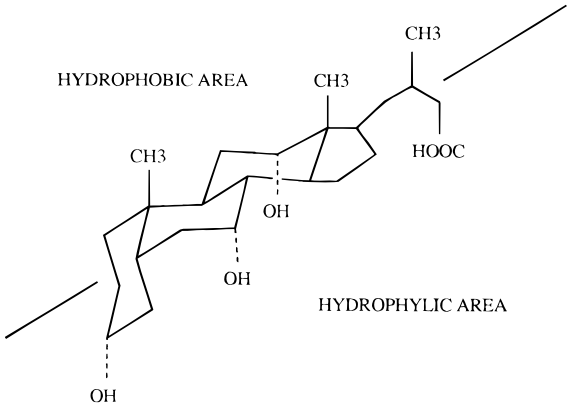

Figure 2. Structure formula of cholic acid indicating respectively the hydrophilic and hydrophobic parts of the molecule.

Fisher[4] assumed the initial formation of small aggregates through hydrogen bonds. In spite of numerous experimental results, their model of aggregation was strongly marshaled by Zana,[5] who threw doubts on the existence of hydrogen bonding in the first step of micellization. Different models were successively proposed involving intermolecular hydrogen bonding in the formation of helical complexes.[6−8] However, very little is known about their behavior at very low bile salt concentration.

The present work is therefore devoted to the experimental study of the self-association patterns of bile salts at concentrations below 0.5 vol % NaDC. Different experimental techniques have been used, namely, SANS, QELS, conductivity, viscometry, and time domain reflectometry (TDR). Important parameters of the present work are concentration, pH, and temperature. Though the existence of critical micellar concentrations (cmc's) is not clear in previous studies,[9−14] we will show that two cmc's are accurately determined, depending both on pH and temperature. Our results are also in favor of elongated aggregates (rodlike shape) whose sizes are strongly pH dependent. Furthermore, it is worth emphasizing that a gel phase transition is identified below pH 7.5.

Experimental Procedures

Sample Preparation. 99% pure sodium deoxycholate was supplied by Merck and used without further purification. A solution of 5 vol % NaDC dissolved in 10 mM Tris buffer (tris-(hydroxymethyl)aminomethane, Tris) with a pH confined within the range 8−10 was obtained by titration with HCl and by continuous stirring before being left to equilibrate. Samples of NaDC in D_2O solutions were prepared and kept at 5 °C in a cold room before measurements to prevent any growth of undesirable organisms or bacteria in the solution. The preparation of a broad range of NaDC samples was obtained by a sequence of successive dilutions of a certain amount of Tris buffer adjusted at the pH of interest. The next step consists in placing the solutions into small glass cuvettes of appropriate thickness.

The Tris buffer is a solution capable of maintaining the pH at some fairly constant value even when small amounts of acid or base are added. Tris was supplied by Sigma under the appelation of Trizma. This compound will produce a pH in solution of approximately pH 4.7, but at this pH, Tris has little if any buffering capacity. However, blending Trizma HCl with Trizma base will produce any desired pH between 6 and 11.

During the preparation of concentrated batches of NaDC, bile salts have shown huge rises of pH accompanied by the formation of large micellar complexes in some cases. This phenomenon leads to the conclusion that hydrogen ions are partially removed from the solution. This effect may be related to the spontaneous micelle-forming properties of NaDC and greatly favored when lowering the pH. It has been pointed out in preliminary studies[6] that the absorption of hydrogen ions was correlated with the extend to which the complexes were broken-up by simply stirring. The pH was therefore adjusted afterward by adding directly a slight amount of carbonate-free NaOH or HCl in NaDC solution placed in a small beaker fitted with electrodes for pH measurements and with a magnetic stirrer.

A pH decrease of the NaDC solution tends to convert it into a gel even from quite dilute solution. The conversion of solution to gel seems to occur through a micelle phase composed of small amounts of pure NaDC. Then, in order to dissolve these complexes, it has been necessary to increase the temperature up to 60 °C and to stir continuously to a final steady viscosity. The phase boundary between the liquid and the gel phase is located at pH 7.5 ± 0.1. Two other prerequisites of importance are the effects of temperature and concentration on pH. It is known for instance that Tris solution has a significant temperature coefficient. As the temperature of the solution decreases from 25 down to 5 °C, the pH will increase an average of 0.03 pH unit per degree. Similarly, as the temperature increases from 25 up to 37 °C, the pH will decrease an average of 0.025 pH unit per degree. Furthermore, it appears that conventional pH meters using porous glass electrodes provide spurious measurements when using Tris solutions. This is explained as being caused by a reaction taking place between Tris and the linen fiber junction of the reference electrode, resulting in high liquid-junction potentials and long equilibration time. Therefore, in order to obtain pH measurements of good validity and reproducibility we used a Twin pH B-112 device in complement to our conventional pH apparatus. This pH meter uses a plate glass electrode sensor warranting a pH range confined between 2 and 12 with ±0.1 pH of repeatability. Measurements can be realized both by immersion in the solution of interest and by dropping a sample over the area of the sensor.

Finally we have to emphasize that neutron-scattering experiments have been performed by using heavy water, D_2O, whereas most of the other experiments have been performed on samples diluted by using low-conductivity ultrapure H_2O from a Millipore apparatus. In order to check the consistency of the experimental procedure, some measurements of the line width and of the shear viscosity have also been performed using D_2O as solvent. No significant differences were observed when comparing the experimental data obtained with the two solvents.

Electrical Conductivity Measurements. Electrical conductivity measurements were carried out both at low frequencies from a few hertz up to 13 MHz with a Hewlett Packard 4192-A impedance analyzer and at high frequency with a time domain

(4) Oakenfull, D. G.; Fisher, L. R. *J. Phys. Chem.* **1978**, *82*, 2443−2445.
(5) Zana, R. *J. Phys. Chem.* **1978**, *82*, 2440−2443.
(6) Blow, D. M.; Rich, A. *Nature* **1959**, *182*, 3566−3571.
(7) Esposito, G.; Giglio E. *J. Phys. Chem.* **1987**, *91*, 356−362.
(8) Campanelli, A. R. J. *Inclusion Phenom. Mol. Recognit. Chem.* **1988**, *7*, 391−400.
(9) Schurtenberger, P.; Mazer, N.; Kanzlg, W. *J. Phys. Chem.* **1983**, *87*, 308.
(10) Kratohvil, J. P.; Hsu, W. P.; Kwok, D. I. *Langmuir* **1986**, *2*, 256−258.
(11) Gupta, P. M.; Srivastava, S. N. *Agra Univ. J. Res.* **1979**, *28*, 143−152.
(12) Kawamura, H.; Manabe, M. *Niihama Kogyo Koto Senmon Gakko Kiyo, Rikogaku-hen* **1989**, *25*, 86−93.
(13) Mukerjee, P. *J. Pharm. Sci.* **1974**, *63*, 972−976.
(14) Roda; Hofmann; Mysels. *J. Biol. Chem.* **1983**, 258.

reflectometer. Both instruments were driven by a Macintosh IICI via an IEEE 488 interface. We use an advanced graphical programming language originally released for Macintosh computers. The LABVIEW software supplied by National Instrument allows us to operate systems, drive devices, and feature highly interactive plottings as well as data analysis. The cells used are Hewlett Packard air lines of different lengths (from 2 to 20 cm), made of two gold-coated copper coaxial cylinders and extensively tested in previous TDR and conductivity measurements. The cell is temperature controlled to within ±0.02 °C within the temperature range from 10 to 50 °C by water circulation generated by an Hubert T-300 cryothermostat.

The time domain reflectometry (TDR) method was used to characterize the dielectric properties of NaDC at higher frequencies, from about 20 MHz up to a few gigahertz, in order to compare our results with those obtained with the impedance bridge. A TDR apparatus[15] consists of a pulse generator and a sampling head which includes four test channels and a coaxial line. The 20 ps rising time voltage pulse generated by the step generator (Hewlett Packard 54121-A) is propagated through a coaxial line. At the interface of the air guide with the medium a part of the pulse will be reflected and a part will be transmitted in this medium. This part is in turn reflected at the end of the cell, producing multiple reflections which are displayed with the incident pulse on the sampling oscilloscope (Hewlett Packard 54120-T) of bandwith 18 GHz. From the comparison between the incident and the multiple reflected pulses, we can deduce the electrical conductivity of the sample.[16] Calibration of the impedance bridge and of the TDR has been achieved by using standard NaCl and KCl solutions. Our conductivity determinations of these aqueous solutions for different salt concentrations compare very well with previous investigations[17] and show a relative accuracy and reproducibility of about ±3%.

Dynamic Light Scattering and Viscosity. Quasi-elastic light scattering experiments (QELS) were performed using a Sematec high-precision goniometer. The sample, whose temperature was controlled to within ±0.02 °C, was irradiated by a Spectra Physics Ar^+ laser operating at a wavelength of 514.5 nm. The light scattered at an angle θ was collected by a very low noise phototube (EMI 9853) whose output feeds a homemade 128 channel real time clipped intensity correlator.[18] In a light scattering experiment the transfer wave vector Q is given by $Q = (4\pi n/\lambda)\sin(\theta/2)$, where n is the refractive index of the solution at laser wave length λ and θ is the scattering angle. The refractive index n was measured as a function of concentration and temperature, at a wavelength of 514.5 nm, using a Pulfrich refractometer. It differs only slightly from the one of pure water at the same temperature. According to the values that can be practically obtained for the scattering angle without introducing any spurious scattering, Q ranged from 1×10^{-3} to 3×10^{-3} Å^{-1}. The intensities scattered by the NaDC water solutions were always small in the concentration range we used. Therefore special care was taken to reduce as much as possible spurious scattering by filtering the solutions on Millipore filters and by insuring a good index matching between the sample and the bath in which it was embedded.

The viscosity of the samples we studied by QELS was measured as a function of composition, temperature, and pH, by using a calibrated Ubelhode viscometer immersed in a large temperature-controlled (±0.02 °C) water bath. The relative accuracy of the measurements was better than ±1%.

Small-Angle Neutron Scattering. Small-angle neutron scattering (SANS) experiments were conducted at the Risø National Laboratory of Denmark. The spectrometer of Risø allows coverage of scattering vectors Q ranging from 0.002 up to 0.6 Å^{-1} with variable neutron wavelength resolution. The 6 m long collimation section consists of one fixed and five movable 1 m sections in which nickel-coated neutron guides can be inserted individually by controlled pneumatic cylinders, allowing the neutron source point to be moved in 1 m increments from 1 to 6 m from the sample position. The SANS monochromator, which consists of a mechanical velocity selector with a variable speed drive and tilt angle, allows us to access the neutron's wavelength from 3 up to 24 Å with a resolution of 9−18%. Most of the results presented below were obtained by selecting 3 and 6 Å neutrons with sample to detector distances of respectively 1 and 3 m. The neutron resolution used was $\Delta\lambda/\lambda = 0.18$, and the neutron beam collimation was determined by the pinhole sizes of 16 and 8 mm diameter at the source and sample positions of interest. In the present experiment the wave vector Q ranged from 10^{-2} up to 0.6 Å^{-1}. The scattering data were previously normalized with respect to H_2O and corrected for background. From this experiment we can deduce the absolute differential cross section per unit scattering volume $d\Sigma(Q)/d\Omega$ as a function of the magnitude of the scattering vector Q. We will derive a theoretical description for the scattering from self-assembled NaDC globular and rodlike micelles. Computer modeling has been realized on Unix work stations by using a nonlinear least squares procedure controlled by the so-called χ^2 test of goodness of fit.

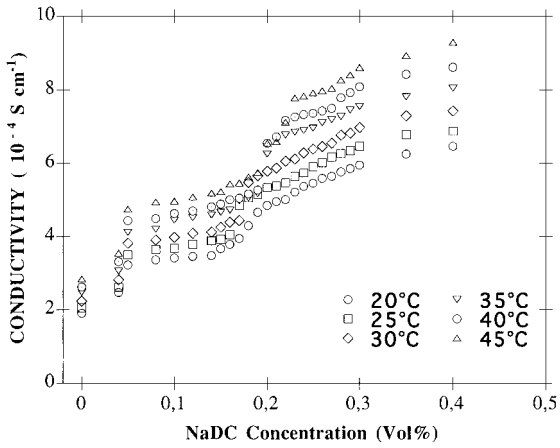

Figure 3. Plot of the low-frequency electrical conductivity versus NaDC concentration at constant pH 9 for different temperatures.

Experimental Results and Discussion

Figure 3 shows a plot of the low-frequency electrical conductivity σ versus concentration at constant pH 9 and various temperatures ranging from 20 to 45 °C. No significant differences were observed between low-frequency data obtained with the impedance bridge and high-frequency data inferred from TDR experiments. This similarity between both measurements indicates that relaxation frequencies should be located at very high frequency. The electrical conductivity is increasing with both temperature and concentration (Figure 3). However for each temperature we studied, a plateau is observed. The lower bound of the plateau is temperature independent and located close to 0.05 vol % of NaDC, whereas the upper bound is found to be temperature dependent, increasing from 0.16 vol % NaDC at 20 °C up to 0.22 vol % NaDC at 45 °C.

Viscosity and QELS experiments were performed on samples whose bile salt concentrations ranged from 0.02 vol % (0.5 mM) up to 0.5 vol % (12.5 mM) at the same pH. The reduced viscosity η_R, defined by

$$\eta_R = \frac{\eta - \eta_0}{C\eta_0} \quad (1)$$

where η and η_0 are respectively the actual viscosity of the solution and that of pure water at the same temperature and C is the composition, is depicted in Figure 4. Below a threshold which can be estimated to be 1.3×10^{-3} g cm^{-3} at pH 8, and 1.5×10^{-3} g cm^{-3} at pH 9, the reduced viscosity is that of water to within experimental error. Above this

(15) Cole, R. H.; Berberian, J. G. *J. Appl. Phys.* **1989**, *66*, 793−802.
(16) Boned, C.; Peyrelasse, J. *J. Phys. E: Sci. Instrum.* **1982**, *15*, 534−537.
(17) Rosen, D.; Bignall, R.; Wisse, J. D. M.; Van Der Drift, A. C. M. *J. Phys. E: Sci. Instrum.* **1969**, *2*, 22−28.
(18) Chen, S. H.; Yip, S. *Spectroscopy in Biology and Chemistry*; Academic Press: New York, 1974.

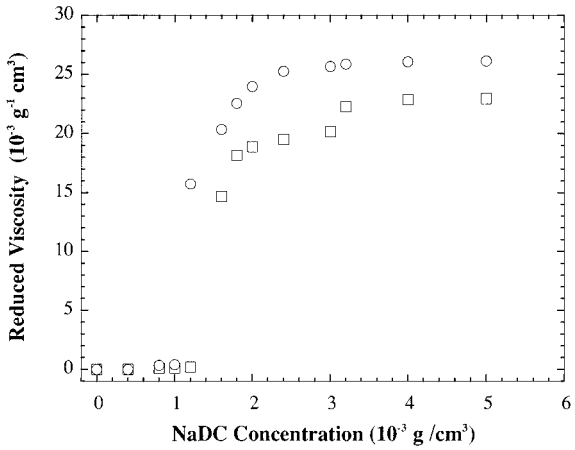

Figure 4. Plot of the reduced viscosity versus NaDC concentration for pH 8.0 and 9.0 at $T = 25$ °C.

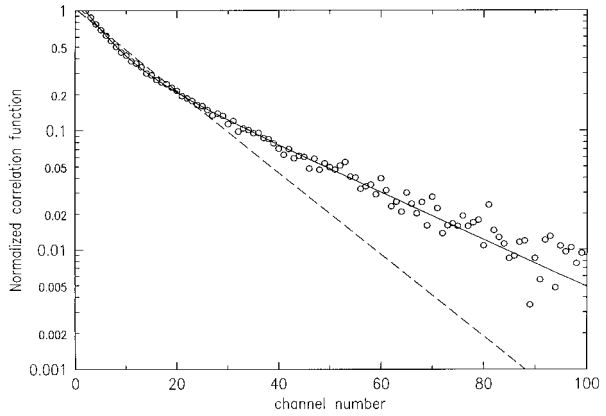

Figure 5. Single- and double-exponential analysis of the normalized intensity correlation function for a solution at 0.16 vol % NaDC (4 mM NaDC) at pH 9.

threshold, a steep increase of η_R is observed. For concentrations larger than 2.5×10^{-3} g cm^{-3}, η_R saturates to a value of the order of 26 g^{-1} cm^3 at pH 8 and 24 g^{-1} cm^3 at pH 9.

At NaDC concentrations below 0.05 vol %, the scattered intensity time correlation function $G(Q,t)$ is essentially flat, reflecting the thermal diffusion of the continuous water medium. The characteristic time of this phenomenon is very short, typically of the order of 0.1 ns, and outside the possibilities of the correlator. Frequently we observed a noisy correlation function of small amplitude on a very large uncorrelated background. This function, which was characterized by a long correlation time, probably reflected the presence of small dust particles which were not completely removed by filtration. Above this threshold, which is the same as the one observed by electrical conductivity and viscosity measurements, the structure of $G(Q,t)$ is considerably improved, showing the presence of mesoscopic aggregates in the solutions of interest. A typical normalized $G(Q,t)$ is depicted as a function of the delay time in Figure 5.

To analyze our QELS data, we first assume the correlation function to be described by a single exponential decay which characterizes the diffusion process of monodispersed dilute spheres:

$$G(Q,t) = A \exp\left[-\frac{2t}{\tau}\right] + B \qquad (2)$$

where τ is the characteristic relaxation time, A is a constant depending on the geometry of the experiment, and B is the amplitude of the uncorrelated background. The factor

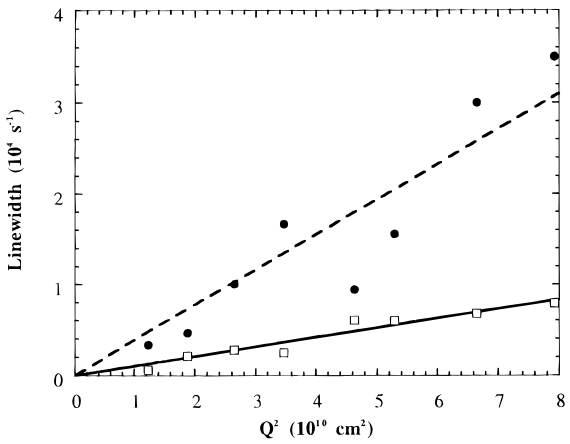

Figure 6. Plot of the relaxation rates deduced from QELS as a function of Q^2 at the concentration 0.1 vol % NaDC (2.5 mM NaDC) and pH 9. The full circles are related to the fast relaxation process whereas the squares are related to the slow one.

2 denotes an homodyne configuration. As shown in Figure 5, a fit of the measured correlation function to a single exponential decay provides systematic errors.

A sum of two exponentials which would be connected to two well defined relaxion processes was then used. In that case the intensity correlation function reads

$$G(Q,t) = \left[A_1 \exp\left(-\frac{t}{\tau_1}\right) + A_2 \exp\left(-\frac{t}{\tau_2}\right)\right]^2 + B \qquad (3)$$

where A_1 and A_2 are the amplitudes of the two relaxation processes characterized by the relaxation times τ_1 and τ_2. Good fits are achieved (Figure 5), leading to two well defined correlation times. For a diffusion process, the line widths Γ_1 and Γ_2, which are the inverse of τ_1 and τ_2, should vary as Q^2, i.e. $\Gamma_i = D_i Q^2$, where D_i is the diffusion coefficient characterizing the ith process. This diffusive behavior is rather well verified by the slow and the fast processes, as shown in Figure 6. At pH 9 for instance, the diffusion coefficients are respectively $D_1 = (6.0 \pm 0.2) \times 10^{-8}$ cm^2 s^{-1} and $D_2 = (4.0 \pm 0.1) \times 10^{-7}$ cm^2 s^{-1}. For a sphere of radius R imbedded into a solvent of shear viscosity η, the translational diffusion coefficient D is given by the Stokes−Einstein formula

$$D = \frac{k_B T}{6\pi\eta R} \qquad (4)$$

where k_B is the Boltzmann constant and T is the absolute temperature. From eq 4 D_1 would correspond to that of a sphere having a diameter typically of the order of 600 Å whereas D_2 would correspond to that of a sphere having a diameter nearly 90 Å. The cumulants method which has also been used provides results having a standard deviation greater than those of the two exponential fits. Nevertheless the first cumulant leads to values of the diffusion coefficient close to the larger one.

In order to confirm the micellization process, we first collected SANS data for samples at different NaDC compositions at a constant value of pH = 9.0. Absolute values of the differential cross section $d\Sigma(Q)/d\Omega$ corrected for solvent scattering and normalized with respect to water are plotted as a function of Q in Figure 7. For NaDC concentrations lower than 0.18 vol % the differential cross section is independent of Q, whereas a structured differential cross section having a well defined maximum is observed for higher values of the NaDC concentration. According to these experimental results, it is clear that mesoscopic size micellar aggregates exist at a concentra-

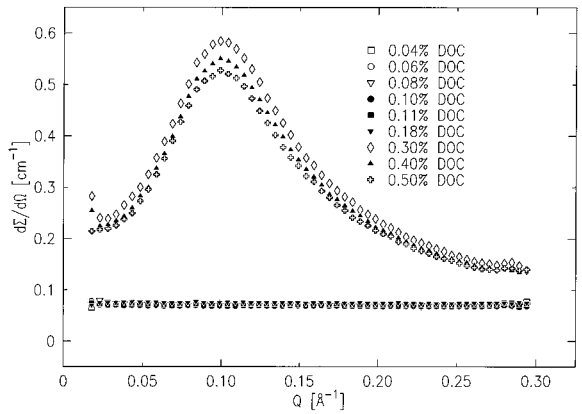

Figure 7. Absolute differential cross-section $d\Sigma/d\Omega$ (cm^{-1}) measured by SANS as a function of the transfer wave vector Q for samples having different NaDC compositions.

tion larger than 0.18 vol % of NaDC corresponding to the second cmc measured by electrical conductivity. Accounting for the sensitivity of neutron scattering experiments, it is however not certain that micellar aggregates are absent at lower NaDC concentrations, but their number density might be too low to be detected.

In order to deduce the shape of the aggregates (at sufficient NaDC concentration), the experimental values of the differential cross section $d\Sigma(Q)/d\Omega$, obtained at different pD and NaDC concentrations, have been fitted to the theoretical scattering functions respectively relevant for monodispersed hard spheres, polydispersed hard spheres having a Schultz type size distribution function, ellipsoids, and rigid rods. These theoretical functions will be given in what follows. The contribution of the ith particle to the scattering can be written in terms of a form factor $F_i(Q)$ which depends only on the shape of the colloidal particle when the scattering density is uniform, leading to[19,20]

$$\frac{d\Sigma(Q)}{d\Omega} = \frac{1}{V}\left\langle \sum_{j=1}^{N}\sum_{k=1}^{N} F_j(Q)\, F_k^*(Q)\, e^{i\vec{Q}(\vec{R}_j - R_k)} \right\rangle \qquad (5)$$

where the brackets denote an ensemble average. The differential cross section of monodispersed spherical particles having the same form factor $F_i(Q)$ is therefore proportional to the product of three terms (eq 6):

$$\frac{d\Sigma(Q)}{d\Omega} = n_p P(Q)\, S(Q) \qquad (6)$$

the particle density n_p, the interparticle structure factor $S(Q)$, and the intraparticle structure factor $P(Q)$ which provides structural information. This term depends upon both the shape of the particle and the distribution of atomic species within it and is given by the following relation:

$$P(Q) = \langle |F(Q)|^2 \rangle \qquad (7)$$

Physically $S(Q)$ represents the positional relationship between the scattering particles and $P(Q)$ their structural information. For polydisperse nonspherical particles, the form factor cannot be factorized out and the differential scattering cross section takes a different form (eq 8):

$$\frac{d\Sigma(Q)}{d\Omega} = n_p P(Q)[1 + \beta(S(Q) - 1)] \qquad (8)$$

where

$$\beta = \frac{\langle |F(Q)| \rangle^2}{\langle |F(Q)^2| \rangle} \qquad (9)$$

The goal of the analysis of neutron scattering data is therefore to feature good models for the intraparticle factor $P(Q)$ which provides structural information.

The formalism presented above has been extended to some common shapes and thus provides the form factors of spherical, ellipsoidal, and rodlike molecular aggregates in the case of monodisperse and polydisperse systems. For uniform spheres it is possible to calculate the form factor, which reads

$$F(Q) = v\Delta\rho \frac{3J_1(QR)}{QR} \qquad (10)$$

In this expression $\Delta\rho = \rho_1 - \rho_s$, where ρ_1 and ρ_s are respectively the scattering densities of the sphere of radius R and of the solvent, v is the volume of the sphere, and $J_1(x)$ is the first-order spherical Bessel function given by

$$J_1(QR) = \frac{\sin(QR) - QR\cos(QR)}{(QR)^2} \qquad (11)$$

The form factor for an ellipsoid scattering particle is given by

$$F(Q,\mu) = \Delta\rho v \frac{3J_1(y)}{y} \qquad (12)$$

If we denote a and b as being respectively the semimajor and semiminor axes of the ellipsoid, we have

$$y = Q\sqrt{a^2(1-\mu^2) + b^2\mu^2} \qquad (13)$$

where μ is the cosine of the angle between $\vec{Q}$ and the Z axis of the ellipsoid.

The form factor for a rigid rod with length L and radius R is given by the expression

$$F(Q,\mu) = \frac{\sin\left(\frac{QL\mu}{2}\right)}{\frac{QL\mu}{2}} \frac{2j_1(QR\sqrt{1-\mu^2})}{QR\sqrt{1-\mu^2}} \qquad (14)$$

where $j_1(x)$ is the first-order Bessel function. Finally, the form factor can be calculated numerically from the following expression

$$P(Q) = \langle [F(Q,\mu)]^2 \rangle = \int_0^1 [F(Q,\mu)]^2\, d\mu \qquad (15)$$

Data analysis based on a nonlinear least squares method to fit successively experimental results to monodispersed hard spheres, ellipsoids, polydispersed spheres having a Schultz size distribution, and rodlike models reveals first a common feature. Particles present in D_2O solutions of 0.5 vol % NaDC become smaller when we increase the pD from the sol/gel phase transition at pD 7.5 (let us recall that for this transition pH = pD up to pD 10). Their major axis (or radius) markedly decreases, leading to the assumption that, upon increasing pD, interparticle interactions become less important, preventing molecules from associating.

(19) Cheu, E.; Chuan, F.; Chen, S. H. *J. Phys. Chem.* **1986**, *90*, 4179−4187.
(20) Chen, S. H. *Annu. Rev. Phys. Chem.* **1986**, *37*, 351−399.
(21) Rouch, J.; Tartaglia, P.; Chen, S. H. *Phys. Rev. Lett.* **1993**, *71*, 1947.

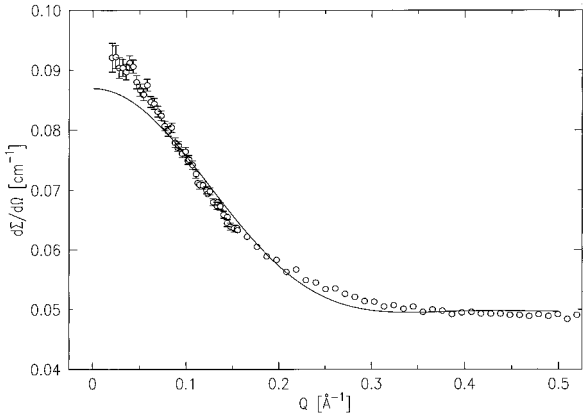

Figure 8. SANS absolute differential cross section for 0.5 vol % NaDC in D_2O at pD 9.6. The circles are experimental data whereas the full line is the best fit to monodispersed hard spheres.

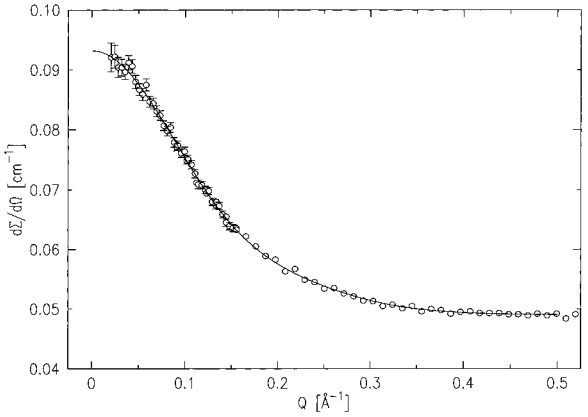

Figure 9. Same as Figure 8 but the full line is the best fit to monodispersed hard rods (eq 14). Very similar results are obtained when the experimental data are fitted to ellipsoids (eq 12).

Let us discuss now in more detail results we obtained when fitting to experiments the various theoretical forms of the structure factor. On one hand, attempts to fit experimental data to monodispersed hard spheres (Figure 8) give unphysical particle dimensions or very bad χ^2 values corresponding to strong systematic deviations from experimental results. Systematic deviations are also observed when fitting data to polydispersed hard sphere systems. On the other hand, the quality of the fit is considerably enhanced if ellipsoidal (eq 12) or cylindrical models (eq 14) are fitted to the data (Figure 9). However because of the shape of the NaDC molecule, the micelle is more likely to have a cylindrical shape than to be a prolate ellipsoid of revolution. The cylindrical model (eq 14), which assumes a homogeneous population, appears adequate for solutions whose pD ≥ 7.5, and confirms the rather structural monodispersity of this micellar system above the second cmc (cmc_2), revealed by conductivity measurements.

Our investigations suggest that rodlike aggregates have considerably elongated when decreasing the pD (Figure 10). From the fits of the data to the rodlike model over a broad pD range, the rod length L increases from (43 ± 3) Å at pD 11 up to (161 ± 5) Å at pD 7.5, whereas at the same time the radius increases from (8 ± 1) Å up to (16 ± 1) Å. Thus the process of enlargement when decreasing the pD continues to be observed until the formation of a transparent gel phase below pD 7.5 (Figure 10 and Table 1). At the boundary with the liquid phase, the gel phase is made of the entanglement of approximately 160 Å length

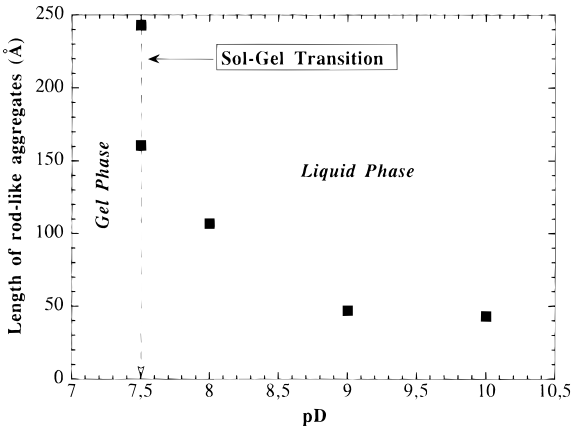

Figure 10. Rod length as a function of the pD of the solution. The vertical dashed line shows the phase transition from liquid to gel which takes place at pD 7.5.

Table 1. Results from Fitting SANS Data to Monodispersed Rods for Various Values of pD[a]

pD	R (Å)	L (Å)
7.5	17.0 ± 0.2	151 ± 7
8.1	8.6 ± 0.1	46 ± 1
8.5	8.2 ± 0.2	42 ± 1
9.6	8.0 ± 0.2	40 ± 1

[a] The sol/gel transition occurs at pD 7.5.

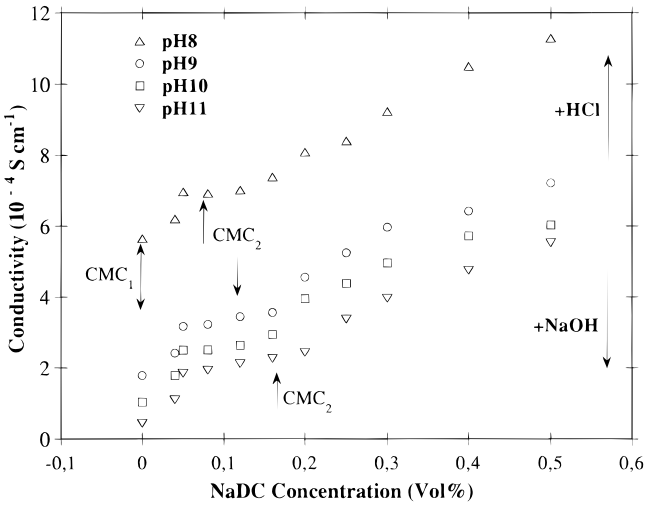

Figure 11. Low-frequency electrical conductivity versus bile salt concentration for different pH values, at T = 20 °C.

and 32 Å diameter rods. Morphological changes occurring on NaDC micelles are therefore strongly pD dependent and show a specific reversibility. It is worth noting that such morphological transformations have been observed when performing QELS and conductivity experiments.

As suggested by QELS, aggregates of mesoscopic size exist only above a critical composition of 0.05 vol % NaDC. This is confirmed by electrical conductivity and viscosity measurements, which show an abrupt change in the slope of plots versus concentration, as shown in Figures 3 and 4. In Figure 11, we have plotted the electrical conductivity versus concentration at constant temperature (T = 20 °C) for different pH values. This plot also clearly reveals the occurrence of a first aggregation mechanism above a characteristic bile salt concentration of the order of 0.06 vol %, independent from pH. A second pH-dependent cmc (cmc_2) is evidenced at higher concentration. At pH 8, cmc_2 occurs at a salt concentration of about 0.12 vol %, whereas it is observed at 0.20 vol % at pH 11. Esposito and Giglio[7] reported results from SAXS experiments as well as ESR

measurements in the domain of high concentration, i.e. above cmc_2. At a pH value fixed just above the one corresponding to the gel phase transition, they observed the presence of helical associations due to the combination of hydrogen bonds and hydrophobic effects. The length of the helix is found to be 116 Å, and the radius is within the range from 9 to 12 Å. SANS experiments do not allow us to make any distinction between an helical shape of the micelles and a cylindrical conformation. We can therefore conclude that the values we are presently reporting are in agreement with those published in ref 7.

As far as QELS is concerned, two discrete relaxation processes are compatible with our experimental data. The diffusion coefficients given above for the two processes differ by a factor ranging from 10 at low concentration to 5 at higher concentrations. A double-exponential behavior is usually expected for a rodlike system undergoing translational and rotational motions.[22] In this case the scattered field correlation function $C(Q,t)$ is given by

$$C(Q,t) = S_0(QL)\exp(-Q^2Dt) + S_1(QL)\exp[-(Q^2D + 6D_R)t] + \ldots \quad (16)$$

where L is the rod length, D_R is the rotational diffusion coefficient, and $S_0(QL)$ and $S_1(QL)$ are the amplitude factors. According to Kubota and Shu,[23] these amplitudes read

$$S_0(QL) = \left(\frac{2}{QL}\right)^2\left[\int_0^{QL/2}\left[\frac{\sin z}{z}\right]dz\right]^2 \quad (17)$$

$$S_1(QL) = \left(\frac{5}{(QL)^2}\right)\left[-3J_1\left(\frac{QL}{2}\right) + \int_0^{QL}\frac{\sin z}{z}\,dz\right]^2 \quad (18)$$

In the case of light scattered by rather small objects ($QL < 1$), expressions 17 and 18 can be expanded:

$$S_0(QL) \approx 1 - \left(\frac{QL}{6}\right)^2 + \ldots \quad (19)$$

$$S_0(QL) \approx \frac{(QL)^4}{720} \quad (20)$$

In our experimental situation (rods of about 100 Å length), numerical applications give S_0 nearly one and S_1 almost zero. In this case it is experimentally impossible to detect any influence of the rotational diffusion. This result is in agreement with Jamieson and Southwick's[24] predictions showing that a reasonable determination of the rotational diffusion coefficient is only possible when the product of the length of the rod L and the transfer wave vector Q is larger than six. This is indeed not the case here. We therefore believe that the bimodal distribution we observe is associated to two different types of aggregates in the solution. The process we observed at short time, corresponding to the larger diffusion coefficient, is connected to the translational diffusion of an equivalent sphere inscribing the cylinder. The slow process corresponds probably to spurious scattering arising from larger dust particles which have not been totally eliminated by filtration. Indeed the diffusion coefficient we observed is similar to the one measured in some experiments for the pure solvent. Nevertheless, our data are not inconsistent with the presence in the solution of small polydispersed micelles, containing a small number of NaDC units. These molecular entities are two small to be seen by SANS and by QELS, as reported by Zana[25] and Esposito and Giglio.[7]

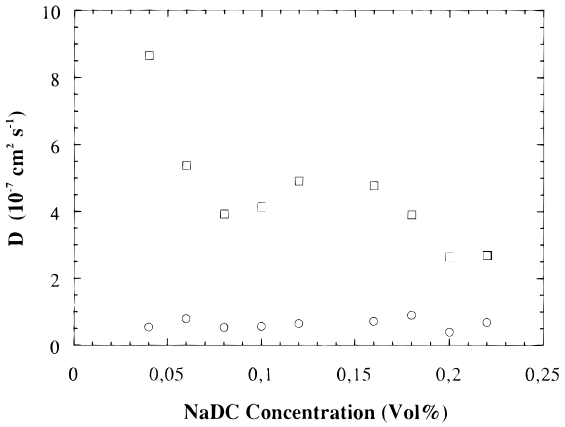

Figure 12. Plot of the diffusion coefficients as a function of the concentration of NaDC at pH = 9.0.

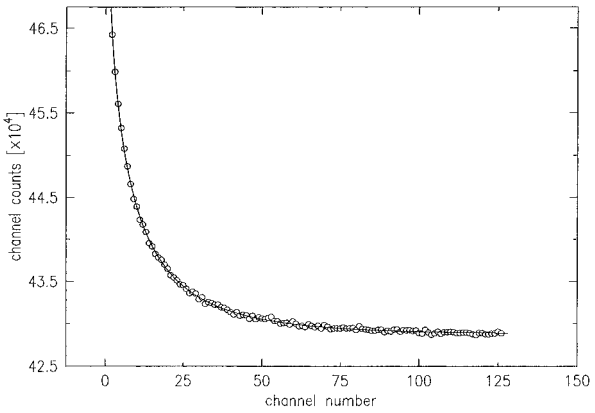

Figure 13. QELS scattered intensity correlation function of 0.16 vol % NaDC (4 mM NaDC) at pH 9. The symbols are experimental data whereas the full line is the best fit to a stretched exponential.

At constant pH, for compositions between the two cmc's corresponding to the plateau value of the electrical conductivity (Figures 3 and 11), the diffusion coefficient D_2 of the fast process inferred from QELS is almost independent of composition and is of the order 4×10^{-7} cm^2 s^{-1} (Figure 12). Let us recall that this value corresponds to micellar aggregates equivalent to a sphere roughly 90 Å in diameter. Moreover the relative amplitude associated with the slow process strongly decreases, leading to an apparent decrease of the overall polydispersity of the system, in agreement with reports of Kratohvil[10] and Esposito and Giglio.[7] At compositions above 0.3 vol % NaDC, the data can be rather accurately fitted to a single exponential. The diffusion coefficient we extract from the fit is similar to the D_2 deduced for compositions in between the two cmc's. This result can be accounted for by the fact that, at high bile salt concentration, the scattering is dominated by the micelles whose number density is rather large. The relative amplitude of the long-time tail of the correlation function becomes negligible, leading to a quasi-monodispersed system.

Let us go back to electrical conductivity data. According to the general shape of conductivity versus concentration plots, the molecular aggregation associated with the plateau seems to occur in two stages (Figures 3 and 12).

(22) Zero, K.; Pecora, R. *Macromolecules* **1982**, *15*, 87.
(23) Kubota, K.; Shu, B. *Biopolymers* **1983**, *22*, 1461−1487.
(24) Jamieson, M.; Southwick, J. G. *Faraday Symp. Chem. Soc.* **1983**, *18*, 131−143.
(25) Zana, R. *J. Phys. Chem.* **1985**, *89*, 1687−1690.
(26) Park, J. W.; Chung, H. *Bull. Korean Chem. Soc.* **1987**, *8*, 118−122.

The first step of the association leads to an expected increase in conductivity. It is worth recalling that this first process of micellization shows a sharp cmc which is temperature independent. The break in the slope of the conductivity versus concentration curve for compositions larger than 0.05 vol % NaDC indicates a transition in the behavior of the solution. It may be accounted for by the fact that the bile salt molecules associate to form micelles, as a result of which the number of free ions and counterions is lowered. Therefore, this slowdown in the slope may be explained by a lower mobility of the associated molecules in solution and the partial absorption of counterions (screening phenomena) on the micellar surface. From a thermodynamical point of view, the phase separation model of micellization described by Fendler and Fendler[27] relates the free energy change ΔG of micellization to the critical micellar concentration cmc by

$$\Delta G = RT \ln(\text{cmc}) \tag{21}$$

where R is the molar gas constant. The enthalpy and entropy changes of micellization, respectively ΔH and ΔS, can be calculated in turn from the following relationships:[27]

$$\Delta H = \frac{\mathrm{d}(\Delta G/T)}{\mathrm{d}(1/T)} \tag{22}$$

$$\Delta S = \frac{1}{T}(\Delta H - \Delta G) \tag{23}$$

As far as the primary micellization process is concerned, ΔG_1 calculated from eq 21, with $\text{cmc}_1 = 1.90 \times 10^{-3}$ mol of NaDC, is estimated to be $\Delta G_1 = -(16.5 \pm 0.5)$ kJ mol^{-1}. This negative value indicating the spontaneity of the process, is in agreement with the one, -15.5 kJ mol^{-1}, obtained by Park and Chung[26] from the study of the fluorescence spectrum of pyrene in NaDC solutions. The enthalpy change ΔH inferred from eq 22 is zero, since the first cmc (cmc_1) is practically temperature independent. This leads to the conclusion that there is no net change in the number or strength of hydrogen bonds in the solution. On the other hand, the entropy variation, $\Delta S = 55$ J K^{-1} mol^{-1}, is strongly positive, a finding also consistent with the Park and Chung[26] data, i.e. $\Delta S = 35$ J K^{-1} mol^{-1}. This highly positive value of ΔS is probably due to a structural modification of the system. This result is a manifestation of the hydrophobic effect.[28] The thermodynamic parameters of NaDC primary micellization are similar to those observed in aqueous solutions of ordinary aliphatic surfactant.

The second discontinuity in the conductivity slope has been associated with a second cmc, cmc_2. As a result of the temperature (or pH) dependence of cmc_2, thermodynamic parameters revealed a different behavior of NaDC at higher concentration in aqueous solution. The enthalpy and entropy changes per mole of primary micelle, respectively ΔH and ΔS, calculated according to the Fendler and Fendler[27] procedure, lead to $\Delta H = -119$ kJ mol^{-1} and $\Delta S = -293$ J K^{-1} mol^{-1} at 35 °C. These values are in agreement with the report of Park and Chung.[26] In view of the large negative enthalpy change, we can conclude that the origin of the secondary micellization cannot be described in terms of a hydrophobic effect. The process is enthalpy driven. According to Park and Chung,[26] when temperature increases, the hydrophobic effect decreases. The formation of secondary micelles reduces the hydrocarbon−water interface and decreases the free energy as well as the enthalpy of the system. This phenomenon is accounted for by hydrogen bonds between solute molecules. At the same time, the entropy of the molecular system decreases on account of the decrease of the solute mobility.

The second cmc, cmc_2, strongly decreases with pH from approximately 0.2 vol % for pH 11 down to 0.1 vol % for pH 8 (Figure 10). When the pH was adjusted too rapidly, we observed in some circumstances the formation of small amounts of unsoluble NaDC and further a sol/gel phase transition depending on the bile salt concentration and temperature of the aqueous solution. The sol/gel phase transition occurs systematically when preparing batches of solutions containing 10 vol % NaDC at pH 8 and 5 vol % NaDC close to pH 7.5. This phase transition is preceded by a dramatic increase of the micellar size when very slightly lowering pH. For instance, the length of the rod measured by SANS for 0.5 vol % NaDC (Figure 9) varies from 150 Å at pH 7.55 up to 250 Å at pH 7.5, leading further to a transparent gel. This transition may be accounted for by the protonation of carboxylate groups, which tends to decrease the electrostatic repulsion between charged NaDC. Such a behavior could be connected in turn to the hydrophobic effect between solvent and solute, since the process of association is typically driven by a positive entropy. These explanations agree with a previous conclusion made by Zana.[5,25] However, more developments are required in order to compare this model with the model of NaDC association established by Small.[3] This author suggests that molecular association of NaDC molecules occurs through intermicellar bonds between hydroxyl groups. These groups are located on the polyhydroxylated concave side of the steroid nucleus and would lead to the association of the so-called "*back to back*" first aggregation pattern in spite of the electrostatic repulsion between the carboxylate groups. Though hydrogen bonding is invoked in several investigations[28−30] made on bile salts, it is worth emphasizing that Zana[5,25] and Mazer et al.[31] do not support this model.

Conclusion

SANS data for NaDC micelles presented above have shown that the "*pH dependent morphological transformations*" observed in the case of low-concentration D_2O−NaDC solutions are also observed for identical pH values by QELS, conductivity, and viscosity measurements. Successive comparisons among the values observed at various pH for NaDC samples clearly indicate an underlying common organizational principle in which the particles grow by elongation above a characteristic critical micellar concentration. Furthermore, several attempts to characterize the structure of bile salt solutions below 0.5 vol % NaDC remained uncertain. The main problem when dealing with the structural determination of sodium deoxycholate molecules below 0.5 vol % NaDC arises from their high polydispersity degree. Because of this high polydispersity characteristic, we had a difficult time constraining the possible models consistent with the data.

As a final comment, let us recall that below a certain value of the pH (pH 7.5) the solution undergoes a sol/gel transition. This abrupt sol/gel transition could be preceded at higher values of pH by cluster formation. Sol/gel transition has been studied by different authors by using QELS techniques. In the case of a chemical gel, Adam et

(27) Fendler, J. H.; Fendler, E. J. *Catalysis in micellar and macromolecular systems*; Academic Press: New York, 1975; pp 35−38.
(28) Tanford, C. *The Hydrophobic Effect*; Wiley: New York, 1979.
(29) Small, D. M. *Adv. Chem. Ser.* **1968**, *84*, 31.
(30) Thomas, D. C.; Christian, S. D. *J. Colloid Interface Sci.* **1980**, *78*, 466.
(31) Maser, N. A. Ph.D. Thesis, MIT, Cambridge, MA, 1978.

al.[32] showed that the intensity correlation function can be cast in an initial single-exponential decay followed by a stretched exponential decay $G(Q,t) \propto \exp[-(D_f Q^2 t)^\beta]$ characterized by a parameter β. As the concentration increases, this mode is better described by a power law in time: $G(Q,t) \propto t^{-\alpha}$. For colloidal silica particles Martin et al.[33] observed an initial exponential decay followed by a power law in time which was cut off by a stretched exponential. This complex behavior of the field correlation was observed recently by Ren et al.[34] in an aqueous solution of gelatin in the dilute and semidilute regime. A single-exponential decay followed at long time by a stretched exponential has also been deduced for interacting fractal objects by Rouch, Tartaglia, and Chen.[21] This function has been shown to be asymptotically valid in the case of complex fluid systems close to a critical point, a percolation phase transition, or a dynamical aggregation process. From the theoretical point of view, scattering by cluster−cluster aggregation has been very recently studied by Sciortino, Belloni, and Tartaglia.[35] These authors showed a maximum in the plot of the scattered intensity as a function of Q, moving toward low Q values as the clustering processes are going on. Besides they also derived the shape of the time decay of the intensity correlation function, which is found to be similar to the one experimentally observed.[36] The abrupt sol/gel transition we observed at pH = 7.5 could be preceded at higher values of pH by cluster formation, which would be reflected in turn by a complex shape of $G(Q,t)$. According to the experimental and theoretical results described above, we tried to cast $G(Q,t)$ in different time domains. We first fitted the short time decay of $G(Q,t)$ to a single exponential. This provides values of the diffusion coefficient corresponding to objects of roughly 90 Å in diameter, growing when lowering pH. It was then almost impossible to fit the data taken at longer time to a power law followed by a stretched exponential decay. On the other hand, at 90° scattering, a reasonably good fit of the total intensity correlation function (except at very short time delay) is achieved with a stretched exponential (Figure 13), the value of the characteristic exponent, $\beta = (0.6 \pm 0.1)$, being almost independent of the NaDC concentration, pH, and temperature. At this point we have to mention that the quality of the fit to a stretched exponential is always lower than that corresponding to the sum of two single exponentials as used in the previous sections of this paper. Besides, we have observed neither a correlation function decaying as a power law nor any maximum of the total scattered intensity for a well defined value of the wave vector Q. We then believe that our dynamical light scattering data are probably polluted by remaining dust particles whose scattering is non-negligible for dilute samples, in particular, in forward scattering at very low Q values. It is therefore quite likely that these dust particles are responsible for the second slow relaxation process. This Q domain is outside the range of our neutron scattering experiments, which are therefore only sensitive to rather small micellar aggregates of NaDC.

Acknowledgment. This work benefited from the use of the small-angle neutron spectrometer of the Risø National Laboratory of Denmark and was supported by the LIP programme. We would like to thank Professors Sciortino and Tartaglia for their very useful comments.

LA960006V

(32) Adam, M.; Delsanti, M.; Munch, J. P.; Durand, D. *Phys. Rev. Lett.* **1988**, *61*, 706.

(33) Martin, J. E.; Wilcoxon, J. P.; Odinek, J. *Phys. Rev.* **1991**, *A43*, 858 and references therein.

(34) Ren, S. Z.; Shi, W. F.; Zhang, W. B.; Sorensen, C. M. *Phys. Rev.* **1992**, *A45*, 2416−2422.

(35) Sciortino, F.; Belloni, A.; Tartaglia, P. *Phys. Rev.* **1995**, *E52*, 4068−4079. For a review on cluster−cluster aggregation, see also: Meakin, P.; Skjeltorp, A. T. *Adv. Phys.* **1993**, *42*, 1−127.

(36) Sciortino, F.; Belloni, A.; Tartaglia. To be published.